Anal Bioanal Chem (2004) 379: 888–899
DOI 10.1007/s00216-004-2664-4

ORIGINAL PAPER

S. E. Maestre · J. L. Todolí · J. M. Mermet

Evaluation of several pneumatic micronebulizers with different designs for use in ICP–AES and ICP–MS. Future directions for further improvement

Received: 12 February 2004 / Revised: 20 April 2004 / Accepted: 30 April 2004 / Published online: 10 June 2004

Abstract This paper reports characterization of the behavior of five pneumatic micronebulizers based on slightly different designs in inductively coupled plasma atomic-emission spectrometry and mass spectrometry (ICP–AES and ICP–MS). Two nebulizers were used as reference nebulizers, a high-efficiency nebulizer (HEN) and a micromist (MM). They were compared with a commercially available PFA (tetrafluoroethylene–perfluoroalkyl vinyl ether copolymer) nebulizer and with two new prototypes called the polymeric pneumatic concentric nebulizer (PMN) and the high-solids micronebulizer (HSM). The dimensions of the nebulizers, the gas back-pressure, and the free liquid uptake rates were measured. The study also included tertiary aerosol drop-size distributions, analyte transport rate, and analytical figures of merit, i.e. sensitivities and limits of detection, both in ICP–AES and ICP–MS. Recoveries for two food solid reference materials were also determined. Overall, the results indicated that the PFA and the HEN nebulizers provided the best results. These two nebulizers delivered a higher mass of analyte to the plasma and showed better sensitivies giving lower limits of detection than the PMN, HSM and MM. The results revealed that the liquid prefilming effect occurring before aerosol production in the PFA nebulizer promoted more efficient interaction of liquid and gas, thus affording good results even though gas back-pressure values could be maintained below 3 bar. In contrast, the HEN had to be operated at about 7 bar under the same conditions. Nebulizer design did not have a relevant effect on the recovery, which confirmed that the spray chamber plays an important role in terms of non-spectroscopic interferences.

Keywords ICP–AES · ICP–MS · Pneumatic micronebulizers · Food analysis · Liquid prefilming

S. E. Maestre (✉) · J. L. Todolí
Departamento de Química Analítica,
Nutrición y Bromatología,
Universidad de Alicante, 03080 Alicante, Spain
E-mail: salvador.maestre@ua.es

J. M. Mermet
Laboratoire des Sciences et Stratégies Analytiques
(CNRS-UMR 5180), Université Claude Bernard-Lyon 1,
69622 Villeurbanne Cedex, France

Introduction

When working with ICP techniques using conventional pneumatic nebulizers at low liquid-delivery rates it can be observed that: the aerosols are rather coarse; and the dead volume is too high. To overcome these problems, several dedicated micronebulizers have been introduced [1]. The common characteristics shown by the micronebulizers are [2]: generation of a stable aerosol at liquid flow rates on the order of several microliters per minute; reduction in the dimensions of the sample capillary; and consequently, very low dead volumes with subsequent mitigation of memory effects. Despite these benefits, the solutions must be filtered, because the presence of solid particles can cause irreversible blocking of the micronebulizer capillary.

The microconcentric nebulizer (MCN) [3], the high efficiency nebulizer (HEN) [4], and the micromist (MM) [5, 6] have been successively made commercially available and have been already studied in detail. The suitability of these nebulizers for the analysis of microsamples has been demonstrated in ICP–AES and in ICP–MS [7, 8]. Due to their low dead volume, they provide narrow peaks in high-performance liquid chromatography–ICP–MS [9] or capillary electrophoresis (CE)–ICP–MS [10, 11] coupling. As regards comparative studies, it has been shown that the HEN provides better analytical figures of merit than MM and MCN, because it generates finer primary aerosols than the other two systems [12]. In contrast, the MM is better suited for CZE–ICP–MS coupling, because, unlike the HEN, a make-up gas in the spray chamber is not necessary [13].

Additional pneumatic micronebulizers have appeared. The high-efficiency cross-flow micronebulizer (HECFMN) [14, 15] has recently been developed for coupling CE with ICP–MS. Among the most important advantages of this device is that it does not aspirate the solution freely and, thus, it is not necessary to use a make-up solution to compensate for changes in the flow inside the capillary during the analyte-separation step.

In the sonic spray nebulizer (SSN), a capillary is inserted into a chamber that contains a final orifice. A gas stream is introduced into the cavity. Simultaneously, the solution is delivered to the nebulizer and reaches the end of the capillary. The liquid and gas interaction takes place and the aerosol is then generated. With the SSN, the limits of detection are better than for conventional pneumatic nebulizers [16]. A modification of the SSN is the multimicrospray nebulizer (MMSN) [17]. In the MMSN the sample stream is diverted into three different lines. Each line end is centered with respect to an independent orifice through which three argon streams flow at a given total gas flow rate. The gas energy is more efficiently employed in aerosol generation because there are three aerosol generation points. As a consequence, higher analyte transport efficiencies and sensitivities are achieved for the MSSN than for the SSN.

The parallel-path micronebulizer has been used for the introduction of liquid samples in plasma spectrometry [18, 19]. In this particular design, the liquid and gas streams are aligned with each other. According to the manufacturer this nebulizer does not suffer from blocking when working with high salt content solutions or slurries. Furthermore, it is suitable for working with CE–ICP coupling.

Although the oscillating capillary nebulizer (OCN) [20] also consists of two concentric silica capillaries, it cannot be considered as a classical pneumatic design. In the OCN, liquid goes along the central capillary whereas gas flows through the area left between the two capillaries. The gas stream induces liquid capillary oscillations that promote aerosol generation. The OCN provides better results than pneumatic concentric micronebulizers [21].

The aim of the work described in this paper was to test the analytical performance of three new pneumatic micronebulizers, one made of PFA (tetrafluoroethylene–perfluoroalkyl vinyl ether copolymer) and two prototypes, one made of glass and another made of polymer, neither of which was yet commercialized. These three nebulizers were compared with two conventional micronebulizers previously studied, the HEN and the MM. Some characteristics of the nebulizers are discussed. All five systems were evaluated by determination of tertiary aerosol properties, analyte transport, and ICP–AES and ICP–MS analytical figures of merit. Two reference food materials were analyzed to evaluate the extent of interferences as a function of liquid flow rate and nebulizer design.

Experimental

Nebulizers and spray chambers used

Because they have been extensively studied, a HEN (Meinhard Glass Products, Santa Ana, CA, USA) and an MM (Glass Expansion, Australia, Model AR30-1-FM005) were used as reference nebulizers. Three additional micronebulizers were also tested. Figure 1a shows a picture of a PFA nebulizer [22] (PFA-ST micronebulizer, CPI International, The Netherlands). Apparently, it is similar to a concentric nebulizer. However, close inspection of the nebulizer tip reveals that the sample capillary is recessed with regard to the nebulizer bore (schematic diagram of the nebulizer tip, Fig. 1a). The aerosol generation principle is different from that of conventional concentric nebulizers. In this case the gas stream is accelerated as it goes through the nebulizer cone. Simultaneously, the liquid solution is deposited on the inner walls of the nebulizer where gas–liquid interaction begins. A process called liquid prefilming then occurs. Liquid prefilming is widely known and used in engineering applications of atomizers [23]. As a result, the liquid film becomes thinner and the gas kinetic energy is efficiently transferred to the liquid. In a different system called the high-solids micronebulizer (HSM; from Microglass of Colorado Quality Scientific Glassware) presented in Fig. 1b, an impact surface is placed just in front of the gas exit where the aerosol is generated. The liquid stream emerges through an upper conduction and moves downward until it reaches the gas orifice. The aerosol is generated and immediately impacts against this surface. As a result, its trajectory deviates as shown in Fig. 1b. Finally, Fig. 1c shows a picture and a schematic diagram of another polymeric micronebulizer (PMN) used in this work. This nebulizer was provided by Sci-Tek Instruments (UK). In this case, prefilming of the aerosol also occurs as the sample is deposited on the inner walls of the nebulizer.

Table 1 shows the critical dimensions of the nebulizers used in this work. The gas-exit cross-sectional area, A_g, was obtained (in mm^2) by applying the following equation [24]:

$$A_g = B\frac{Q_g}{p_0} \quad (1)$$

where Q_g is the gas flow rate (in L s^{-1}) and p_0 is the absolute pressure (in atm). In Eq. 1, B is a parameter that depends on gas physical properties such as density, specific heat at constant volume, and pressure and temperature [24].

For comparison purposes the critical dimensions of a Glass-Expansion conventional pneumatic concentric nebulizer are also included in Table 1. It can be observed that the main modifications incorporated in the micronebulizers compared with conventional ones consist of reduction of both the inner diameter and wall thickness

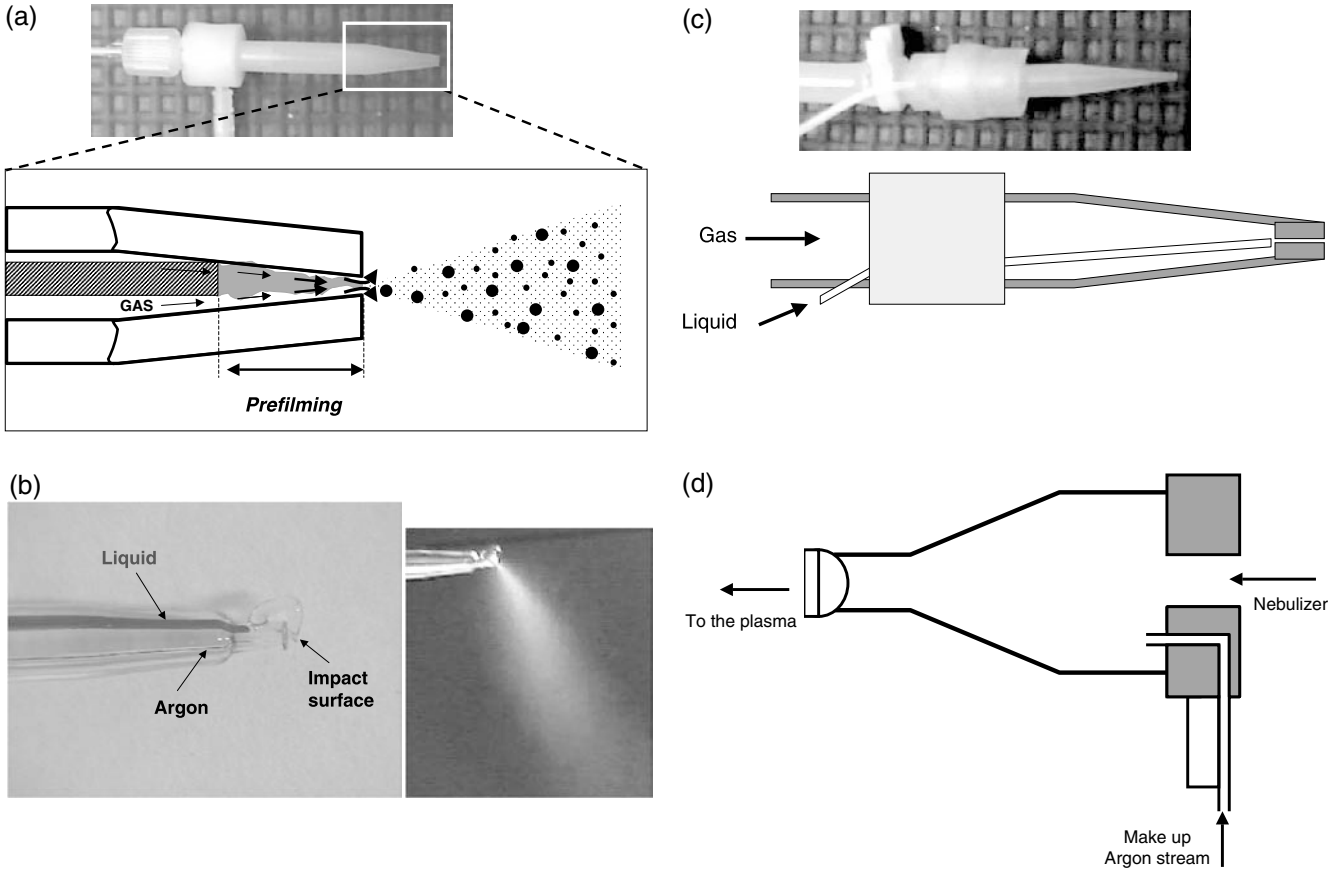

Fig. 1 Pictures of the PFA nebulizer with a schematic diagram of the nozzle (**a**); the HSM, together with the aerosol (**b**); the PMN with a schematic diagram of the nozzle (**c**); and the single-pass spray chamber equipped with an inlet for an argon carrier stream (**d**)

of the sample capillary. In addition, for the HEN and HSM, the gas-exit cross-sectional area is lower than for the other systems, which means that a higher gas pressure is required to achieve a given gas flow rate. From Table 1, it can be seen that this critical dimension follows the increasing order: HEN < HSM < MM < PFA < PMN.

Two spray chambers were used: a glass 50 cm^3 cyclonic spray chamber (Glass Expansion), and a horizontally operated polypropylene 30 cm^3 single pass spray chamber. Figure 1d shows a schematic diagram of the latter design. In this particular case, a make-up gas stream was used.

Aerosol and analyte transport measurements

The finest fraction of tertiary aerosol, i.e. the aerosol that leaves the spray chamber, was measured for each nebulizer. In this work the volume drop-size distributions were obtained. These experiments were carried out by means of a scanning electromobility particle sizer (SPMS, TSI Incorporated, St Paul, MN, USA). Operating conditions were the same as those described in previous studies [25].

The analyte transport rates were obtained by a direct method, i.e. by collecting the aerosol on a glass fiber filter (type A/E, 47 mm diameter, 0.3 μm pore size, Gelman Sciences, Ann Arbor, MI, USA) placed above the spray chamber. A 500-μg mL^{-1} Mn solution was nebulized. The Mn retained on the filters after a period of 10 min (for experiments performed at 30 μL min^{-1}) and 20 min (for those at 10 μL min^{-1}) was extracted by

Table 1 Critical dimensions of the pneumatic micronebulizers used in this work

Nebulizer	Gas-exit cross-sectional area (mm^2)	Liquid capillary inner diameter (μm)	Liquid capillary wall thickness (μm)
High-efficiency nebulizer	0.008	100	30
High-solids micronebulizer	0.011	500	–
Micromist	0.018	140	50
Polymeric micronebulizer	0.030	–	–
PFA nebulizer	0.021	270	–
Conventional concentric nebulizer	0.028	400	60

washing them with a 1.0% (*w*/*w*) hot nitric acid solution. The total solution volume was adjusted to 25 mL with a volumetric flask. Finally, the Mn concentration was determined in each solution by flame atomic absorption spectrometry.

For these experiments, the cyclonic spray chamber was used.

ICP–AES and MS Instruments

The measurement of the ICP–AES intensities was performed by adapting each nebulizer to the cyclonic spray chamber. A Varian Vista Pro (Australia) axially-viewed spectrometer was used. Table 2 shows the instrumental conditions. The nebulizer (central) gas flow rate was optimized in terms of ICP–AES sensitivity for the five nebulizers evaluated. A 10-μg mL^{-1} multielement solution was prepared from a 1,000 μg mL^{-1} stock solution (Merck IV). The elements, wavelength and E_{sum} for ionic lines (or E_{exc} for atomic lines) are gathered in Table 3. The ICP–MS measurements, in turn, were carried out by means of a VG PQ ExCell instrument. In this case, the single-pass conical spray chamber (Fig. 1d) was used. Table 2 also includes the operating conditions used for these experiments. Because of the high gas back-pressure required for the HEN and HSM at the optimum central flow rate (i.e. 1.05 L min^{-1}) a make-up gas stream was needed in ICP–MS.

Analysis of solid certified materials

Two different food CRMs were analyzed, mussel tissue (CRM 278R) and bovine liver (CRM 185R). The digestion procedure followed has been described elsewhere [26]. Once the digestion was accomplished, samples were filtered and the total volume of the resulting solution was adjusted to 50 mL with concentrated nitric acid. This was done in order to ensure that the matrix (i.e., nitric acid and inorganic salts) would cause significant interferences. Because the concentration of many elements was very low, 10 g of each sample solution were spiked, after the digestion step, by adding 20 μL of the 1,000 μg mL^{-1} multielement solution to match the sensitivity of ICP–AES. The composition of the spiked reference materials is summarized in Table 4. Finally, the samples were analyzed with the ICP–AES instrument by using plain water standards. Recoveries were calculated by dividing the concentration found by that certified. For the ICP–MS experiments, after the digestion step, the spiked samples were diluted 200-fold with Suprapure® nitric acid. The final acid concentration was

Table 2 Spectrometer operating conditions

ICP–AES Instrument	
RF power	1.35 kW
External gas flow rate	15 L min^{-1}
Intermediate gas flow rate	1.5 L min^{-1}
Central gas flow rate	0.75 L min^{-1}
Read time	1 s
ICP–MS instrument	
Plasma	
RF power	Variable
External gas	13.5 L min^{-1}
Intermediate gas	0.82 L min^{-1}
Central gas	0.75 L min^{-1}
Make-up gas	0.3 L min^{-1}
Acquisition parameters	
Mode	Peak jump
Sweeps	10
Dwell time	10 ms
Channels per mass	3
Channels spacing	2
Acquisition time	10 s

Table 3 Elements, wavelength, *and* E_{sum} for ionic lines or E_{exc} for atomic lines

Element	Wavelength (nm)	E_{sum} or E_{exc} (eV)
Al I	308.215	4.02
Ba II	455.403	7.93
Bi I	306.771	4.04
Cd II	214.439	14.77
Co II	228.615	13.70
Cr II	205.560	12.80
Cu I	223.009	6.95
Fe II	238.204	13.07
Mg I	285.213	4.35
Mg II	280.270	12.07
Mn II	257.610	12.25
Ni II	221.648	14.27
Pb II	220.353	14.79
Sr II	216.596	13.26
Zn I	213.857	5.80

Table 4 Concentration of trace elements in the solutions resulting from the CRM treatment

Sample	Element	Concentration referred to solid (μg g^{-1})
Bovine liver (CRM 185R)	Cd[a]	67.2
	Cu[a]	344
	Mn[a]	77.7
	Pb[a]	66.8
	Zn[a]	205
	Co[b]	66.7
	Ni[b]	66.7
	Bi[b]	66.7
	Ba[b]	66.7
	Cr[b]	66.7
Mussel tissue (CRM 278R)	Cd[b]	66.7
	Cu[a]	76.1
	Mn[a]	74.4
	Pb[a]	68.7
	Zn[a]	83.1
	Co[b]	66.7
	Ni[b]	66.7
	Bi[b]	66.7
	Ba[b]	66.7
	Cr[a]	67.4

[a]Certified elements
[b]Added elements

50% (*v*/*v*) for solutions analyzed by ICP–AES and 20% (*v*/*v*) in those analyzed by ICP–MS.

Results and discussion

Nebulizer characterization

An important property of pneumatic nebulizers is the gas back-pressure. Table 5 summarizes the values of the pressure required for the gas stream in order to achieve two different gas flow rates, namely 0.75 L min^{-1} and 1.0 L min^{-1}. It can be observed that values of this property for the HEN and HSM are higher than for the other devices. For these two nebulizers an additional gas line must be used, because commercial spectrometers are usually able to withstand maximum pressure values of about 5 bar. It can also be observed that the back-pressure is higher for the MM than for the PFA; the PNM device requires the lowest gas line pressure to reach a given gas flow rate.

Table 5 also includes the free liquid uptake rate for a flow rate of 0.75 L min^{-1}. It can be observed that this value was lower for the HEN than for the other nebulizers. It is widely known that the lower the inner diameter of the nebulizer sample capillary, the lower the free liquid uptake rate. Following this discussion, Table 5 also shows that the free liquid uptake rate was higher for the MM than for the PFA. However, according to Table 1, the inner diameter of the capillary is higher for the latter nebulizer than for the MM. These results could be accounted for by the higher gas back-pressure required for the MM. Note that the higher the pressure drop between the liquid capillary exit and the solution, the higher the free liquid uptake rate.

Aerosol and analyte transport studies

In a previous study [12] it was found that the HEN provides primary aerosols finer than the MM and the conventional nebulizer. The reason for this trend is that the gas-exit cross-sectional area is smaller and, hence, the gas back-pressure is higher for this system than for the other two nebulizers. As a result, a higher amount of kinetic energy is available for the aerosol production. Other studies have demonstrated that the PFA nebulizer is able to provide finer primary aerosols than the MM [27]. Note that, under the same conditions, the gas back-pressure is lower for the PFA than that for the MM. These results indicate that energy transfer from the gas to the liquid stream is more efficient for the PFA nebulizer. The prefilming effect occurring in the PFA nebulizer could be responsible for the generation of finer aerosols with a lower net amount of kinetic energy.

An interesting property of the aerosol is its spread. Because of the role of the impacts on the chamber walls, in this study the aerosol cone diameters were measured at two different locations, i.e. 5 and 15 mm from the nebulizer nozzle. The data indicated that, among the nebulizers tested, the HSM generated the aerosols with the widest cone, i.e. a cone of 20 and 28 mm diameter 5 and 15 mm, respectively, from the nebulizer tip. The other devices provided aerosol cones with similar dimensions, i.e. cones that ranged between 3 mm diameter for the PFA and 5 mm diameter for the MM, 5 mm from the nebulizer tip, and cone diameters between 8 mm (for the PFA, PNM and HEN) and 10 mm (for the MM) 15 mm from the nebulizer tip. Therefore, the aerosol inertial impacts against the spray chamber inner walls were more significant for the HSM than for the other designs.

The signal finally obtained depends on the tertiary aerosol characteristics. The finest fraction of this aerosol was investigated by coupling the micronebulizers to a cyclonic spray chamber. Figure 2 shows the plot of the submicrometer drop-size distribution for the five micronebulizers studied. It can be observed that there were no remarkable differences between aerosol mean size. Thus, at 10 μL min^{-1} the median of the mass drop-size distributions of sub-micrometer particles (i.e. D_{50}) were 0.44 μm for the HSM and about 0.5 μm for the other nebulizers. The spray chamber was therefore more important than the nebulizers in determining the quality of tertiary aerosols. As the liquid flow-rate increased, no noticeable changes in D_{50} values were found. Thus, at 120 μL min^{-1}, the D_{50} were about 0.4 and 0.45 μm for the HSM and the other devices, respectively. In contrast, changes in the total mass of aerosol leaving the spray chamber were observed to be a function of the nebulizer (Fig. 2 and Table 6). Thus for the HEN and PFA nebulizers this property was higher than for the MM, the PMN and the HSM being the devices that afforded the lowest mass of aerosol transported to the plasma

Table 5 Gas back-pressure and free liquid uptake rates for the different nebulizers tested

Nebulizer	Gas back-pressure (bar)		Free liquid uptake rate (μL min^{-1})[a]
	$Q_g = 0.75$ L min^{-1}	$Q_g = 1.0$ L min^{-1}	
High-efficiency nebulizer	7.5	10	40
High-solids micronebulizer	5.4	7	–
Micromist	3.2	4.2	290
PFA nebulizer	2.4	3.1	160
Polymeric micronebulizer	1.4	2.2	120
Conventional concentric nebulizer	1.5	2.0	1,100

[a]At 0.75 L min^{-1} nebulizer gas flow rate

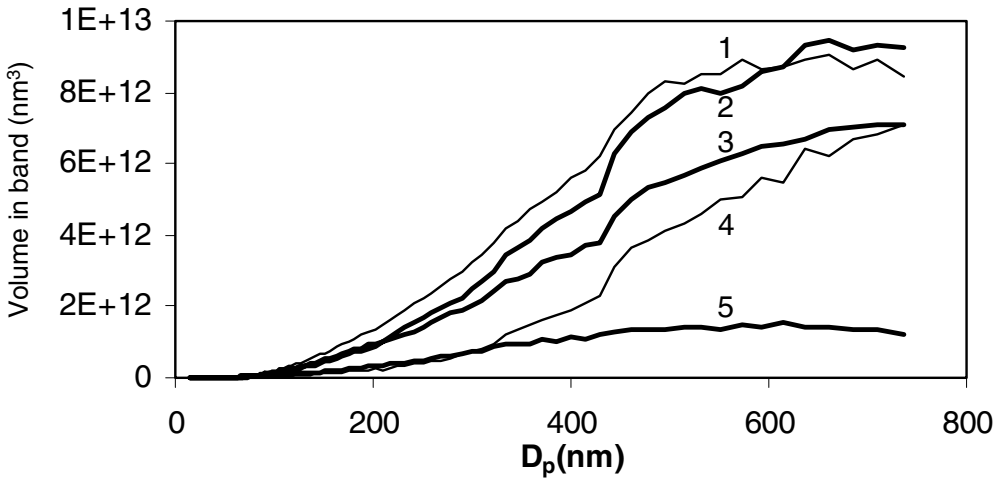

Fig. 2 Frequency volume drop-size distribution curves for the aerosols leaving the cyclonic spray chamber. *1* HEN, *2* PFA nebulizer, *3* MM, *4* PMN, *5* HSM. $Q_g = 0.7$ l/min; $Q_l = 10$ μL min^{-1}

(Fig. 2). This trend was presumably because of the finer primary aerosols generated by the HEN and PFA. The finer the primary aerosols the higher the mass of aerosol transported to the plasma. For the HSM two other factors should also be taken into account—the fact that the aerosol cone was wider than for the other three nebulizers and the evidence that the aerosol was directed against the inner walls of the spray chamber (Fig. 1b).

Table 6 gathers the values of the analyte transport efficiency, ε_n, and the analyte transport rate, W_{tot}. First, it can be observed that, among the systems tested, the HEN and PFA afforded the highest values of ε_n and W_{tot}. The second column of Table 6 includes the results. Good correlation was established in qualitative terms between analyte transport and aerosol concentration. However, quantitatively speaking there was disagreement between W_{tot} (and ε_n) and aerosol concentration. Thus, for example, at 10 μL min^{-1} it can be observed that for the HEN W_{tot} was 6.3 times higher than for the HSM. Meanwhile, the value of the HEN to HSM tertiary aerosol concentration was 5.4. The reason for this discrepancy can be found by considering that an important fraction of the tertiary aerosol was not considered when characterizing it (i.e. droplets with diameters within 0.7 μm and the cut-off diameter whereas W_{tot} represented the total tertiary aerosol.

ICP–AES analytical figures of merit

The sensitivities correlate strongly with the liquid flow rate and the nebulizer tested. Under the conditions tested in this work the emission intensity relative standard deviations ranged from 0.5 to 2%. Figure 3 shows the average relative sensitivity obtained for the PFA, HSM, PNM, and MM micronebulizers operated at four different liquid flow rates. To calculate the average relative sensitivity, the signal found for each of these four nebulizers was divided by those provided by the HEN. This procedure was followed for a set of 14 emission lines. Finally the average value of these relative signals was calculated. As expected from the W_{tot} and ε_n data, the HSM provided lower ICP–AES emission intensities than the other systems tested. At 17 μL min^{-1} both HEN and PFA provided similar sensitivities and up to four times higher than those encountered for the HSM. Qualitatively, these results were in agreement with W_{tot} (Table 6). Nonetheless, the signal improvement factor was lower than that for analyte transport. This disagreement could be explained by the fact that positioning the HSM was critical; because the aerosol cone deviated (Fig. 1b), a slight change in the relative position of the tip could severely affect the extent of analyte losses in the spray chamber.

Table 6 Tertiary aerosol concentration, analyte transport efficiency, ε_n, analyte transport rate, W_{tot}, and Mn analytical signal obtained for the different nebulizers tested

Nebulizer	Aerosol concentration (μm^3 cm^{-3})[a]		ε_n (%) and W_{tot}, (μg min^{-1})[b]		Signal for Mn 257.610 nm[a]	
	30 μL min^{-1}	10 μL min^{-1}	30 μL min^{-1}	10 μL min^{-1}	30 μL min^{-1}	10 μL min^{-1}
HSM	17	6.3	14 (0.7)	4 (0.6)	9,258	5,918
PMN	16	10	–	11 (1.7)	15,115	10,039
MM	61	23	30 (1.5)	12 (1.8)	19,156	12,775
PFA	73	30	73 (3.7)	28 (4.2)	27,844	20,702
HEN	79	34	88 (4.5)	26 (3.9)	31,254	23,487

[a]RSD from three measurements $< 3\%$
[b]RSD from three measurements $< 10\%$

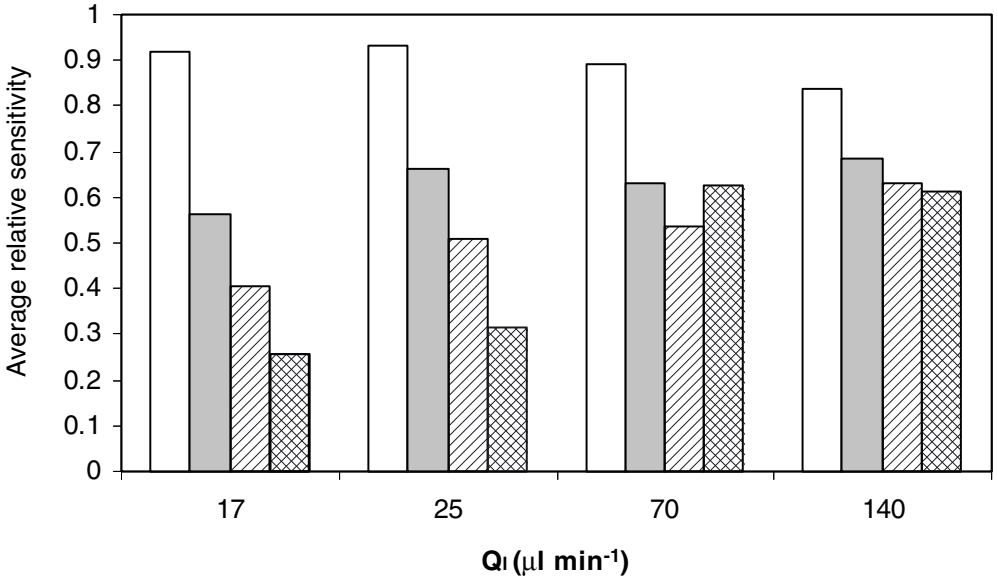

Fig. 3 Average relative sensitivity (i.e. $\text{signal}_{\text{Micronebulizer 1}}/\text{signal}_{\text{HEN}}$ averaged for a set of 14 lines) for the PFA nebulizer (*white bars*), the MM (*grey bars*), the PMN (*dashed bars*), and the HSM (*cross-hatched bars*) for a set of different Q_l. $Q_g = 0.75$ L min^{-1}

Figure 3 shows that for the HSM and PMN the average relative intensity increased as the liquid flow rate was increased (i.e. the signal improvement achieved by use of HEN and PFA decreased as Q_l increased). Thus, for example, at 140 μL min^{-1} liquid flow rate the improvement factor (i.e. average relative signal for the HEN or PFA divided by that for the HSM) dropped to 1.3 and 1.5 for the PFA nebulizer and the HEN, respectively. Therefore, the use of these two nebulizers seemed to be advantageous with respect to the HSM mainly at liquid flow rates of a few tens of microliters per minute.

Limits of detection (LOD) were obtained by following the $3\sigma_B$ criterion, where σ_B is the absolute standard deviation of ten consecutive measurements of the blank. Figure 4 shows the values of LOD for the nebulizers and emission lines tested in this work at two different liquid flow rates. At 17 μL min^{-1} (Fig. 4a) the LOD were lower for the HEN, MM, and PFA nebulizers than for the HSM. The relative average limits of detection were 3.3, 3.2, and 4.9 for the HEN, MM and PFA, respectively. However, at 140 μL min^{-1} (Fig. 4b), the value of the improvement factor was 1.8 irrespective of the nebulizer tested. Again, the results demonstrate that the HSM is not suitable for work at liquid flow rates of the order of several tens of microliters per minute, at least with clean water solutions.

Analysis of food certified reference materials

Once the samples were dissolved, they were analyzed by using plain water standards. The recoveries found for the two food samples are presented in Fig. 5 for the five micronebulizers operated at 17 μL min^{-1}. It can be observed that, in general terms, the recoveries were higher for the HEN and the PFA than for the other three nebulizers. According to these data, the nebulizers providing lower W_{tot} values were those which afforded the lowest recoveries. In general terms, the liquid flow rate did not have a noticeable effect on the recoveries for the different nebulizers. Only the HEN exhibited average recoveries that were slightly lower at 17 μL min^{-1} (55 and 61% for bovine liver and mussel tissue, respectively) than at 140 μL min^{-1} (for which the respective values were 63 and 69%). It has previously been indicated that at low liquid flow rates the interferences caused by inorganic matrices are more severe than at conventional liquid flow rates [25]. This trend, however, is strongly correlated with spray-chamber design and it has proven to be less pronounced for cyclonic than for double-pass spray chambers [28].

ICP–MS studies

As mentioned in the experimental section, the single pass spray chamber was used for the ICP–MS experiments. Usually, this spray chamber is operated with an impact bead placed in front of the nebulizer. However, it was observed that at low liquid flow rates the impact bead induced a sharp drop in the sensitivity because a large fraction of the solution was lost as it impacted against it. Furthermore, the position of the nebulizer nozzle relative to this surface was critical. This is illustrated in Fig. 6 in which the ^{115}In ionic intensity is reported for four different nebulizer positions at four liquid flow rates when the PFA nebulizer was used. The nebulizer has been recessed by 5, 10, and 15 mm relative to the default initial position. It can be seen that the signal sharply increased when the nebulizer was moved back relative to the spray chamber. This caused the nebulizer tip-to-impact surface gap to increase from approximately 5 mm (i.e. the default position) to 20 mm. Then it reached a plateau. Obviously, an increase in this distance enhanced the chance of droplets being transported to the

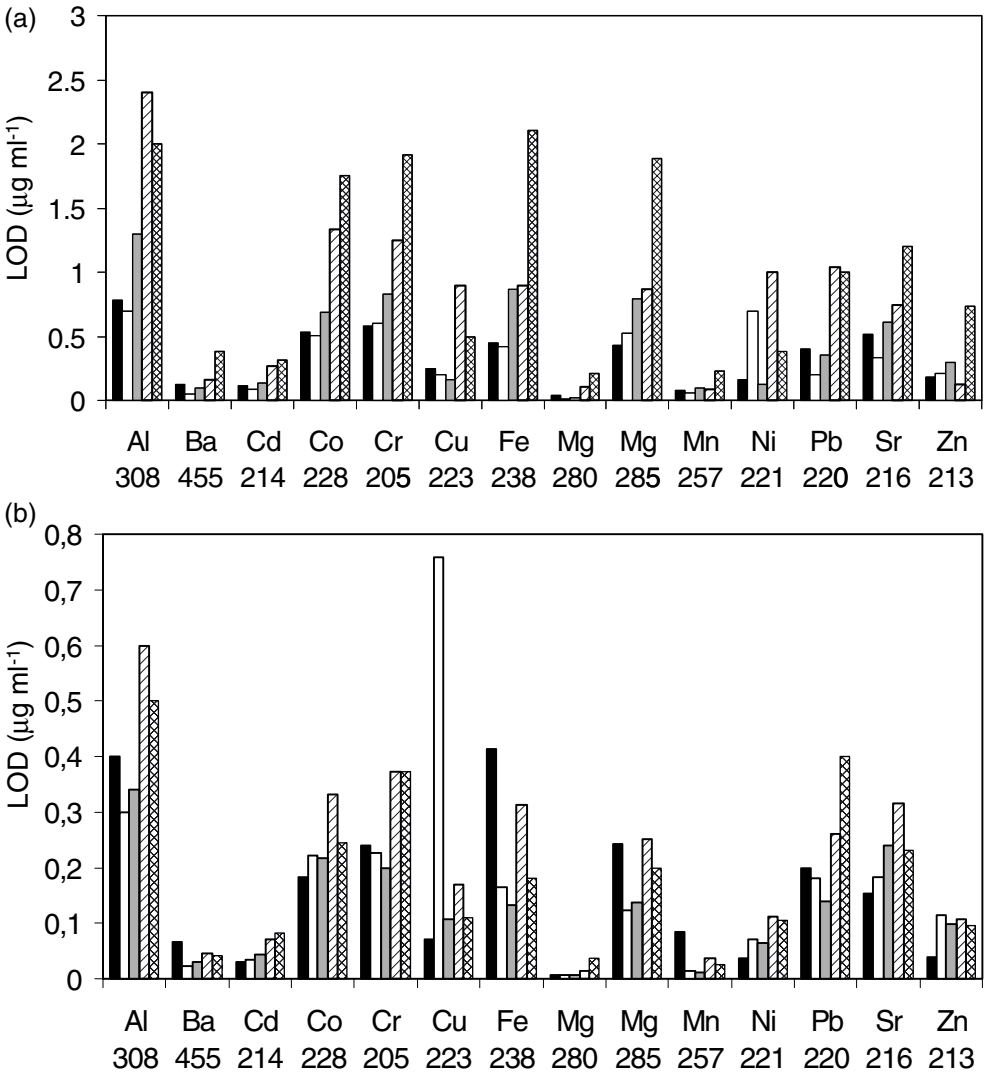

Fig. 4 LOD for the HEN (*black bars*), the PFA nebulizer (*white bars*), the MM (*grey bars*), the PMN (*dashed bars*) and the HSM (*cross-hatched bars*). $Q_l = 17$ µL min^{-1} (**a**); $Q_l = 140$ µL min^{-1} (**b**). $Q_g = 0.75$ L min^{-1}. LOD for Al, Cu, Ni and Pb have been divided by ten in order to scale them

plasma. Note that the cone diameter of the aerosol generated by the nebulizer increased with the distance. As a result, the bead intercepted a lower aerosol volume as the nebulizer was moved back and, hence, the mass of analyte transported towards the plasma went up. Positioning the nebulizers studied at the same distance from the impact bead was difficult because of their different lengths.

For the reasons mentioned above, in this work the impact bead was removed. As Fig. 1d illustrates, a capillary was introduced inside the chamber via the drains to introduce a make-up argon stream. Thus, the nebulizer gas flow rate was kept constant at the same value as used for ICP–AES studies. This was done because for nebulizers such as the HEN and HSM, the pressure required to reach the optimum plasma central gas flow rate, i.e. 1.05 L min^{-1}, was about 10 and 7 bar, respectively. Such high pressure values could make it necessary to use special (perhaps metallic) gas conductors instead of the Tygon and Polyimide tubing employed in this work.

For each nebulizer and liquid flow rate the operating RF power, the ion optics, the torch position and the carrier argon flow rate were optimized by monitoring the ^{115}In signal. The results obtained indicated that the optimum make up argon flow rate was 0.3 L min^{-1}, irrespective of the nebulizer and liquid delivery rate. Nonetheless, the plasma RF power that provided the highest value of the ^{115}In ionic intensity was dependent on the liquid flow rate. Four values of Q_l were tested: 30, 60, 120 and 300 µL min^{-1}. It was found that for the first two values the optimum RF power was 1.2 kW, whereas for the remaining two Q_l values, the highest indium signal was reached at 1.35 kW.

Figure 7 shows the signals found in ICP–MS for the HEN, PFA, MM, and HSM for a set of 13 isotopes covering a wide range of masses. The RSD ($n = 9$) of the signal was always below 5%. As expected from the results discussed in the ICP–AES section, the HEN and PFA nebulizers led to higher ion intensities than the MM and HSM. Because of the characteristics of the aerosol generated by the latter nebulizer (Fig. 1b), a

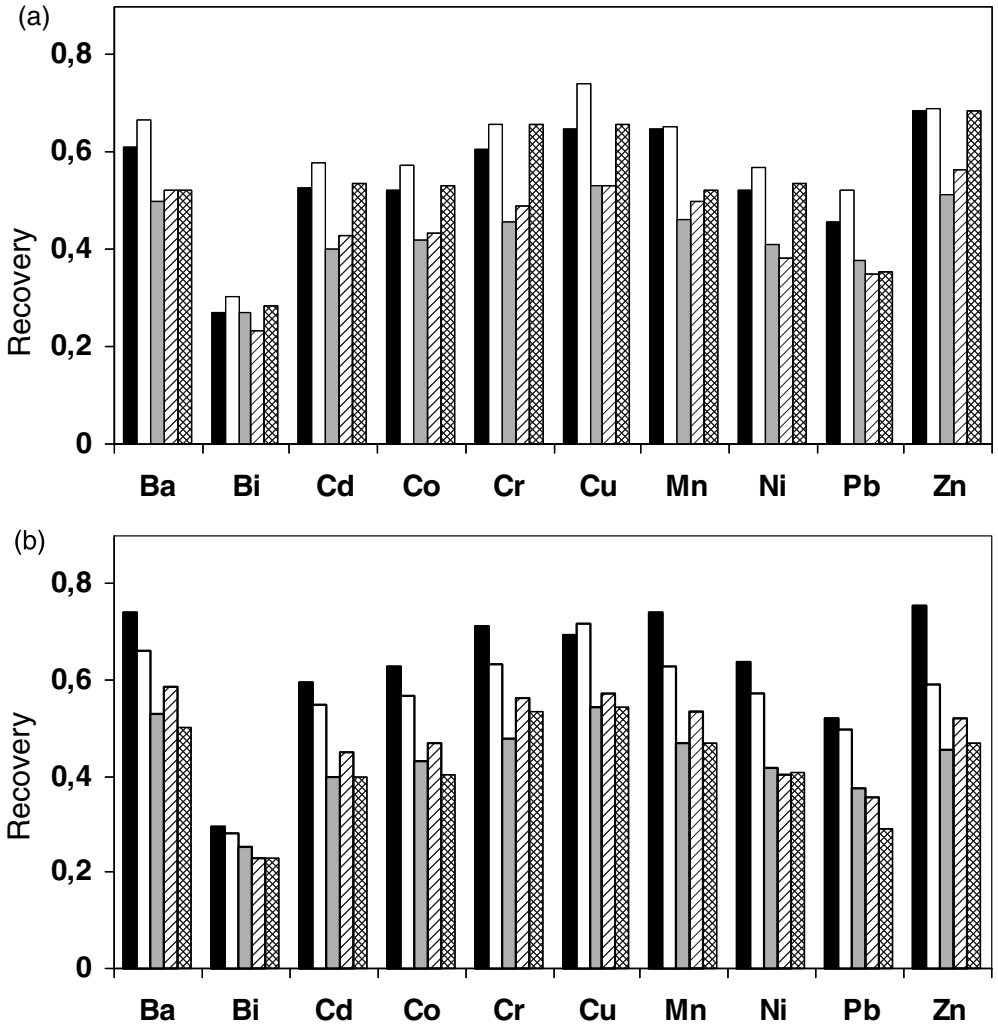

Fig. 5 Recoveries for the different nebulizers obtained at 17 μL min^{-1} for bovine liver (**a**) and mussel tissue (**b**). *Black bars* HEN, *white bars* PFA nebulizer, *grey bars* MM, *dashed bars* PMN, and *crosshatched bars* HSM. $Q_g = 0.75$ L min^{-1}

large fraction of it impacted against the inner walls of the chamber and, hence, the signal was the lowest among the nebulizers tested. At 300 μL min^{-1}, the average signal improvement factors of concentric nebulizers relative to those for the HSM were 2.3 for the HEN and PFA and 1.7 for the MM. However, as in AES, at liquid flow rates of several tens of microliters per minute (e.g. 30 μL min^{-1}) the differences between HEN (or PFA) and HSM were more significant. Under these conditions, the average relative signals (i.e. the signal for HEN or PFA divided by that for the HSM) were 3.5 for these two nebulizers, whereas it was just 1.5 for the MM. These results confirm the suitability of HEN and PFA for analysis of microsamples by ICP–MS.

Doubly charged species and oxide levels were monitored by means of the Ce^{++}/Ce^{+} and CeO^{+}/Ce^{+} ratios, respectively. Globally it was found that these ratios did not change significantly as a function of the nebulizer. Thus, at 60 μL min^{-1} the doubly charged ratios were 1.1, 0.7, 0.8, and 1.7% for the HEN, PFA, MM and HSM, respectively. The corresponding values for the oxide ratios were: 3.4, 2.9, 6.1, and 7% for the same nebulizers. These expected results could be attrib-

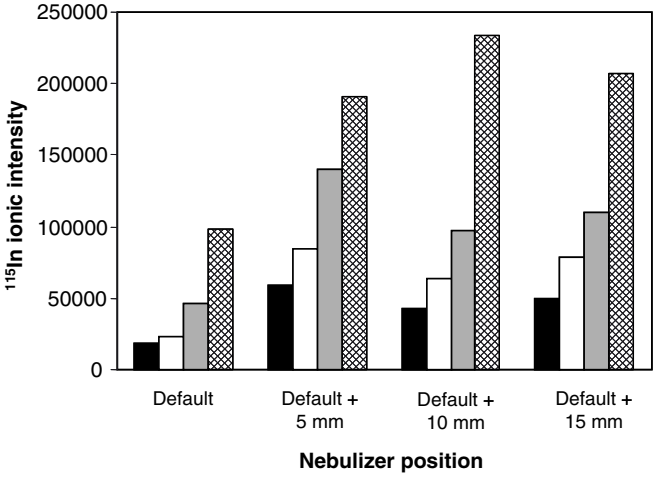

Fig. 6 ^{115}In signal intensity for four different nebulizer positions relative to the impact bead for the PFA nebulizer operated at different liquid flow rates, Q_l. *Black bars* $Q_l = 30$ μL min^{-1}, *white bars* $Q_l = 60$ μL min^{-1}, *grey bars* $Q_l = 120$ μL min^{-1}, *crosshatched bars* $Q_l = 300$ μL min^{-1}. $Q_g = 0.75$ L min^{-1}

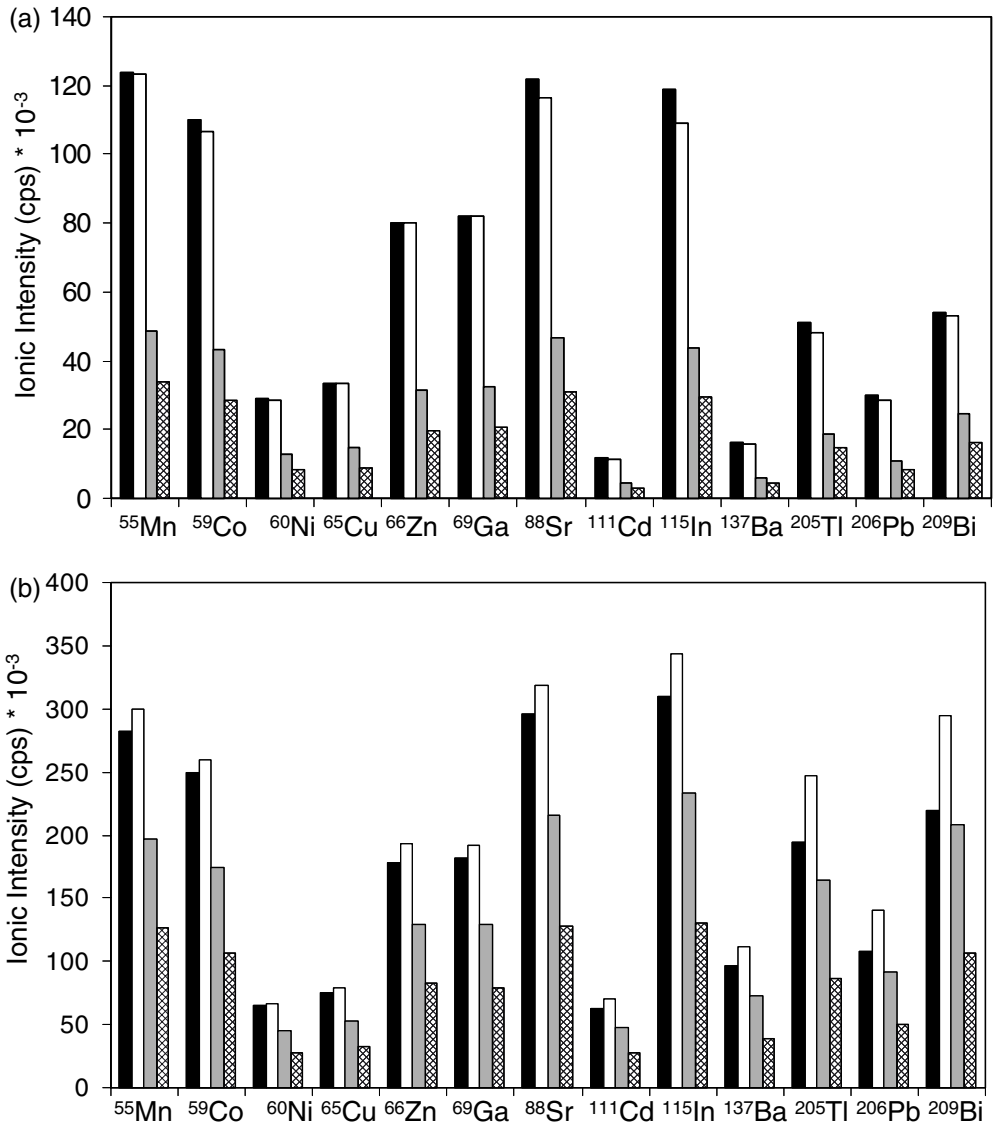

Fig. 7 Signal intensity found for several isotopes for the HEN (*black bars*) the PFA nebulizer (*white bars*) the MM (*grey bars*), and the HSM (*cross-hatched bars*). $Q_l = 30$ μL min^{-1}, RF power = 1.2 kW (**a**) and $Q_l = 300$ μL min^{-1}, RF power = 1.35 kW (**b**). $Q_g = 0.75$ L min^{-1}

uted to the fact that, unlike the amount of analyte, the mass of solvent transported towards the plasma was similar for the four nebulizers tested. The fraction of solution that impacted against the inner walls of the chamber evaporated, at least partially, and the differences in terms of solvent transport as function of the nebulizer were less significant than the effects on W_{tot} [12].

The limits of detection are shown in Fig. 8. According to the data presented in Fig. 8a, the LOD were lower for the three pneumatic concentric nebulizers (the average relative limits of detection were 6.6, 3, and 3.6 for the HEN, PFA, and MM, respectively) than for the HSM. The results obtained for the PFA nebulizer were mainly because of the increase in the blank standard deviation ($n = 20$) relative to those of the other two concentric nebulizers. Meanwhile, at 300 μL min^{-1} (Fig. 8b), the PFA nebulizer seemed to give rise to LOD lower than or similar to those measured for the HEN. The LOD provided by the PFA were, on average, a factor of 3.7 lower than those afforded by the HSM, this factor being 2.9 and 1.1 for the HEN and MM, respectively.

As regards the analysis of the reference food samples, after digestion the resulting solutions were filtered and they were diluted 200-fold with Suprapure nitric acid. The estimated nitric acid concentration in these solutions was 2 mol L^{-1} . The results were quite similar in relative terms to those shown for optical emission. Nebulizer design had little effect on the recoveries obtained.

Future improvements

The results obtained from the comparison made in this work indicate that PFA and HEN are better suited to the analysis of microsamples by atomic spectrometry than the MM, HSM, and PMN. The results obtained with the PFA device are similar to those afforded by the

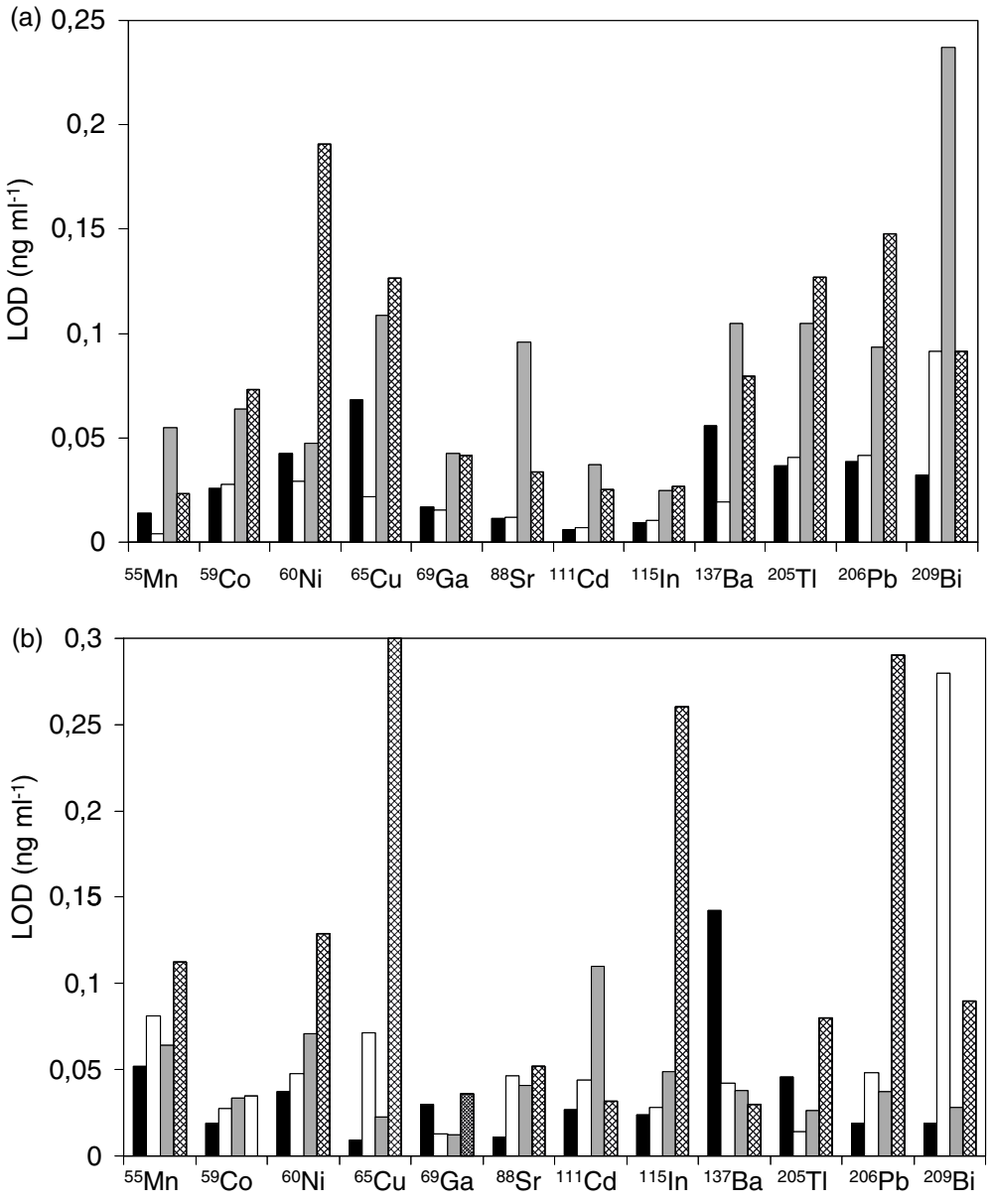

Fig. 8 Limits of detection for several isotopes for the HEN (*black bars*), the PFA nebulizer (*white bars*), the MM (*grey bars*), and the HSM (*cross-hatched bars*). $Q_l = 30$ μL min^{-1}, RF power = 1.2 kW (**a**) and $Q_l = 300$ μL min^{-1}, RF power = 1.35 kW (**b**). $Q_g = 0.75$ L min^{-1}

HEN even though the pressure applied to the argon stream is about a factor of three times lower. This could be explained by considering that the liquid sample prefilming occurring at the tip of the nebulizer enhances liquid–gas interaction. In other words, the gas kinetic energy is more efficiently used in aerosol generation for the PFA than for the HEN. Another advantage of the PFA nebulizer is that it can be adapted to the spectrometer gas line whereas a high pressure gas line should be used for the HEN.

Incorporation of the prefilming effect in the aerosol generation mechanism is beneficial in order to achieve closer and more efficient gas–liquid interaction. As has been demonstrated throughout this work, it improves the characteristics of the aerosols, solution transport to the plasma, and analytical figures of merit in both ICP–AES and ICP–MS. The prefilming leads to a decrease in the liquid vein thickness. Hence, it is possible to increase the nebulizer liquid capillary inner diameter without disturbing the aerosol-generation process. It should, of course, be taken into account that if the inner diameter of the capillary of the nebulizer is too large memory effects will increase. Nevertheless, a compromise i.d. can be used (such as that shown in Table 1 for the PFA or even higher) thus avoiding capillary tip blocking without increasing the severity of memory effects.

Apart from this, the best nebulizer characteristics also depend on the particular application. Thus, in capillary electrophoresis besides the analytical figures of merit an important point that should be considered is whether the nebulizer aspirates the solution freely or not [29]. Nebulizers that do not tend to aspirate the solution are

preferred in order to mitigate changes in laminar flow. According to the data summarized in Table 5, the HEN could be regarded as more appropriate for CE–ICP coupling, because for this system the free liquid uptake rate is lower than for the others. Nonetheless, there still is a given suction effect that should be minimized. In order to reduce it, it would be useful to reduce the velocity of the gas stream at the liquid–gas interaction point. In this way the drop pressure, responsible for the solution aspiration, would decrease. This could be achieved by recessing the nebulizer sample capillary. In the PFA nebulizer the liquid capillary end was located 7 mm from the nebulizer tip. Apparently, this recess was not enough to eliminate the solution suction effect (Table 5). Therefore, either higher capillary recess degrees or nebulizer nozzle cones with high angles should be tested.

The results found for the PFA nebulizer in terms of analytical figures of merit could be further improved by reducing the orifice cross-sectional area. This would require increasing the gas pressure. From theoretical calculations it was concluded that PFA nebulizers with an orifice cross-sectional area 40 and 20% lower than that used in this work (i.e. 1.2×10^{-2} mm^2 and 1.7×10^{-2} mm^2, respectively, instead of 2.1×10^{-2} mm^2 for the PFA nebulizer used in this study) should provide better results in ICP–AES and ICP–MS, respectively. This would give rise to nebulizer tip bores with diameters of 120 and 150 μm, respectively. Presumably, tip-blocking problems would not be observed with such dimensions, whether working with high salt-content solutions or with slurries.

The HSM has been developed for the analysis of high salt-content solutions and slurries. Obviously, despite the low sensitivities and high limits of detection resulting from use of this nebulizer compared with conventional nebulizers, with this kind of sample the HSM would lead to superior performance. Note that for use of the HEN, for instance, every solution must be filtered—otherwise the sample capillary becomes quickly, and sometimes irreversibly, blocked. With the micromist blocking problems are seldom encountered when working with high salt-content solutions; likewise, the PFA can run salty solutions without tip blocking.

Acknowledgements The authors wish to thank Varian Inc. and Varian France for the loan of the ICP–AES instrument and Glass Expansion, Meinhard Glass Products, CPI International, Microglass of Colorado Quality Scientific Glassware and SCI-TEK instruments for providing the nebulizers used in this study.

References

1. Montaser A, Minnich MG, McLean JA, Liu H, Caruso JA, McLeod CW (1998) In: Montaser A (ed) Inductively coupled plasma mass spectrometry. Wiley-VCH, New York
2. McLean JA, Minnich MG, Iacone LA, Liu H, Montaser A (1998) J Anal At Spectrom 13:829–842
3. Packer AP, Gine MF, dos Reis BF, Menegario AA (2001) Anal Chim Acta 438:267–272
4. Olesik JW, Kinzer JA, Harkleroad B (1994) Anal Chem 66:2022–2030
5. Langlois B, Dautheribes JL, Mermet JM (2003) J Anal At Spectrom 18:76–79
6. Todolí JL, Mermet JM (2002) J Anal At Spectrom 17:345–351
7. Vanhaecke F, Holderbeke MV, Moens L, Dams R (1996) J Anal At Spectrom 11:543–548
8. Boulyga SF, Becker JS (2001) Fresenius J Anal Chem 370:612–617
9. Woller A, Garraud H, Boisson J, Dorthe AM, Fodor P, Donard OFX (1998) J Anal At Spectrom 13:141–149
10. Tangen A, Lund W (2000) J Chromatogr A 891:129–138
11. Casiot C, Donard OFX, Potin-Gautier M (2002) Spectrochim Acta Part B 57:173–187
12. Todolí JL, Hernandis V, Canals A, Mermet JM (1999) J Anal At Spectrom 14:1289–1295
13. Alvarez-Llamas G, de-la-Campa MRF, Sanchez MLF, Sanz-Medel A (2002) J Anal At Spectrom 17:655–661
14. Li J, Umemura T, Odake T, Tsunoda K (2001) Anal Chem 73:1416–1424
15. Li J, Umemura T, Odake T, Tsunoda K (2001) Anal Chem 73:5992–5999
16. Huang M, Shirasaki T, Hirabayashi A, Koizuma H (1999) Anal Chem 71:427–432
17. Huang M, Hirabayashi A, Shirasaki T, Koizumi H (2000) Anal Chem 72:2463–2467
18. http://burgenerresearch.com
19. Burgener J (2003) Federation of analytical chemistry and spectroscopy societies, Fort Lauderdale, Paper No. 267
20. Wang L, May SW, Browner RF, Pollock SH (1996) J Anal At Spectrom 11:1137–1146
21. Hoang TT, May SW, Browner RF (2002) J Anal At Spectrom 17:1575–1581
22. Wind M, Wesch H, Lehman WD (2001) Anal Chem 73:3006–3010
23. Lefebvre AH (1989) Atomization and Sprays. Hemisphere, New York
24. Sharp BL (1988) J Anal At Spectrom 3:613–652
25. Todolí JL, Mermet JM, Canals A, Hernandis V (1998) J Anal At Spectrom 13:55–62
26. Todolí JL, Mermet JM (2003) J Anal At Spectrom 18:1185–1191
27. Todolí JL, Maestre SE, Mermet JM (2003) Federation of analytical chemistry and spectroscopy societies, Fort Lauderdale, Paper No. 274
28. Todolí JL, Mermet JM (2000) J Anal At Spectrom 15:863–867
29. Yanes EG, Miller-Ihli NJ (2003) Spectrochim Acta Part B 58:949–955